

Metasurface-Empowered Optical Multiplexing and Multifunction

Shuqi Chen,* Wenwei Liu, Zhancheng Li, Hua Cheng, and Jianguo Tian

Metasurfaces are planar photonic elements composed of subwavelength nanostructures, which can deeply interact with light and exploit new degrees of freedom (DOF) to manipulate optical fields. In the past decade, metasurfaces have drawn great interest from the scientific community due to their profound potential to arbitrarily control light. Here, recent developments of multiplexing and multifunctional metasurfaces, which enable concurrent tasks through a dramatic compact design, are reviewed. The fundamental properties, design strategies, and applications of multiplexing and multifunctional metasurfaces are then discussed. First, recent progress on angular momentum multiplexing, including its behavior under different incident conditions, is considered. Second, a detailed overview of polarization-controlled, wavelength-selective, angle-selective, and reconfigurable multiplexing/multifunctional metasurfaces is provided. Then, the integrated and on-chip design of multifunctional metasurfaces is addressed. Finally, future directions and potential applications are presented.

1. Introduction

Metasurfaces are a class of ultrathin planar optical components proposed in the past decade, which are composed of one or few layers of artificial morphological structures assembled from conventional materials.^[1] By delicate design of structures in each unit cell, metasurfaces can provide an additional phase gradient or surface momentum, which expands the Snell's law to generalized Snell's law.^[2–5] Although metasurfaces are much thinner than 3D metamaterials, they are still capable

of generating outstanding and strong light-matter interactions at the nanoscale. Taking advantages of the abundant resonances between light and structures, such as electric dipole resonances,^[6] magnetic dipole resonances,^[7] toroidal dipole resonances,^[8] metasurfaces can manipulate light with different degrees of freedom (DOF). For example, the coupling strength of light into artificial structures can be utilized to manipulate the amplitude of the wave functions, such as perfect absorbers,^[9,10] structural colors,^[11,12] and asymmetric transmission.^[13,14] The frequency manipulation is known as resonances in different wavelengths such as nonlinear excitation,^[15] or as resonances between two different oscillators, such as Fano resonances^[16–18] and Borrmann resonances.^[19] The phase of the scattered light can be manipulated by metasurfaces


through resonance phase, Pancharatnam-Berry phase, propagation phase, and the detour phase.^[20–27] The Pancharatnam-Berry phase is decided by the symmetry of the nanostructures, and is linearly proportional to the orientation angle of the nanostructures, which enables continuously phase manipulating of metasurfaces.^[28] The detour phase, which originates from the linear relationship between the scattered phase and the displacement of the nanostructure, is also independent of the working wavelengths, and is highly angle-tolerable.^[29] The polarization of the scattered light can also be fully controlled by anisotropic design of nanostructures, which has been utilized to realize polarization conversion^[30–32] and vector beams generation.^[23,33] On the other hand, simultaneous and independent control of different dimensions of optical waves have drawn much attention of the scientific community.^[34–39] Based on the versatile manipulation of different dimensions of optical waves with metasurfaces, researchers have developed massive functional designs such as metalenses,^[40–42] holography,^[43–45] and chiral detection.^[46,47]

Since great achievements have been made to realize customized single functionality in metasurfaces, more and more researchers have focused on integrated design of metasurfaces that can deal with concurrent tasks to form a complete metasurface system, and further to develop integrated photonic nanotechnologies. Multiplexing is a concept in telecommunication and computer networks, which means combining multiple signals into one signal. In the optical metasurfaces platform, multiplexing implies optical communication that consists of different information channels.^[48] Multifunction design is more general than multiplexing, which can integrate different

Prof. S. Chen, Dr. W. Liu, Dr. Z. Li, Prof. H. Cheng, Prof. J. Tian
The Key Laboratory of Weak Light Nonlinear Photonics
Ministry of Education
School of Physics, Teda Institute of Applied Physics, and Renewable
Energy Conversion and Storage Center
Nankai University
Tianjin 300071, China
E-mail: schen@nankai.edu.cn

Prof. S. Chen
The collaborative Innovation Center of Extreme Optics
Shanxi University
Taiyuan, Shanxi 030006, China

Prof. S. Chen
Collaborative Innovation Center of Light Manipulations and Applications
Shandong Normal University
Jinan 250358, China

 The ORCID identification number(s) for the author(s) of this article can be found under <https://doi.org/10.1002/adma.201805912>.

DOI: 10.1002/adma.201805912

functionalities into a single metasurface. Looking back on the past several years, researchers have designed multiplexing and multifunctional metasurfaces with different information channels and functionalities under different DOF (Figure 1). For example, researchers have developed polarization-controlled, wavelength-selective, angle-selective multiplexing/multifunctional metasurfaces, which widely expanded the family of integrated metasurfaces and exploited new fundamental areas of nanophotonic technologies. When integrating different channels or functionalities, segmented, interleaved, harmonic, few-layer designs are most commonly employed.^[49–51] On the other hand, reconfigurable metasurfaces provide an alternative new approach for the realization of optical multiplexing and the integration of different optical functionalities under different time series.^[52]

There are still some challenges in this research field due to some critical issues, such as the lack of multidimensional manipulation of optical waves, the lack of universal design strategy, fabrication limitation, and signal to noise ratio. However, to date a lot of efforts have been made to overcome the challenges and limitations, and researchers have taken a big step toward integrated and on-chip multifunctional metasystems. Here, we present a few particularly exciting research achievements to review the progress of multiplexing and multifunctional metasurfaces. In Section 2, we review the theoretical design of angular momentum multiplexing metasurfaces, and discuss the polarization-controlled, wavelength-selective, angle-selective, reconfigurable, and integrated multiplexing/multifunctional devices from Section 3 to Section 7. In the last section, we provide an outlook on challenges and future research prospects.

2. Angular Momentum Multiplexing Metasurfaces

Angular momentum is commonly used in multiplexing metasurfaces since the angular momentum of light is conserved, even when the light meets a small scatterer during its propagation. Thus, the optical information can be easily described by the topological charges. Maguid et al. summarized three methods to realize multiplexing metasurfaces that can generate several vortex channels,^[49] as shown in Figure 2a,b. For segmented design, each channel is independent and generated from different areas of the device; for interleaved design, the vortex beam channels are also independently designed and the metasurface pattern of each channel is mixed together; whereas for harmonic resonance design, all the channels are simultaneously designed and each nanostructure contains information of all the channels.^[53] The third method has better signal to noise ratio, and higher information density. The harmonic resonance design is realized with Fourier transform of the transmission/reflection function of the metasurfaces

$$|\psi(k)\rangle = \sum_j^N \sum_v^{n_j} \exp\{ikr_v^{(j)} + i\phi_v^{(j)}\} \quad (1)$$

where $r_v^{(j)}$ is the position of v nanostructure, and $\phi_v^{(j)}$ is the phase of the v nanostructure in the j th channel. Thus, all the channels are designed together and the total scattered field $|\psi(k)\rangle$ in k -space



Shuqi Chen is a professor at the Key Laboratory of Weak Light Nonlinear Photonics, Ministry of Education, School of Physics and Teda Institute of Applied Physics, Nankai University, China. He received his joint training Ph.D. degree from the University of Arizona, USA, and Nankai University, China, in 2009. His current research interests include nonlinear optics, phononics and acoustics metasurfaces, and subwavelength electromagnetics.



Wenwei Liu is a doctor at the Key Laboratory of Weak Light Nonlinear Photonics, Ministry of Education, School of Physics and Teda Institute of Applied Physics, Nankai University, China. He received his B.S. degree in theoretical physics and Ph.D. degree in optics from Nankai University. His current research focuses on dielectric metasurfaces.



Zhancheng Li is a doctor at the Key Laboratory of Weak Light Nonlinear Photonics, Ministry of Education, School of Physics and Teda Institute of Applied Physics, Nankai University, China. He received his B.S. degree in materials physics and Ph.D. degree in optics from Nankai University. His current research focuses on chiral metasurfaces.

is obtained. This method not only can realize multiplexing, but also can achieve demultiplexing. As shown in Figure 2c, Li et al. proposed vortex beam multiplexing and demultiplexing with a single metasurface in the visible,^[54] and Zhao et al. demonstrated similar effects with C-shaped ring resonators in the terahertz waveband (Figure 2d).^[55] These designs are based on phase manipulation of the incident light, which suffer from intrinsic noises due to the lack of the intensity information of the Fourier components. Liu et al. proposed a dielectric nanopillar design that can manipulate the transmitted Fourier components with high efficiency, and further can control the intensity ratio of each channel with high accuracy (Figure 2e).^[56]

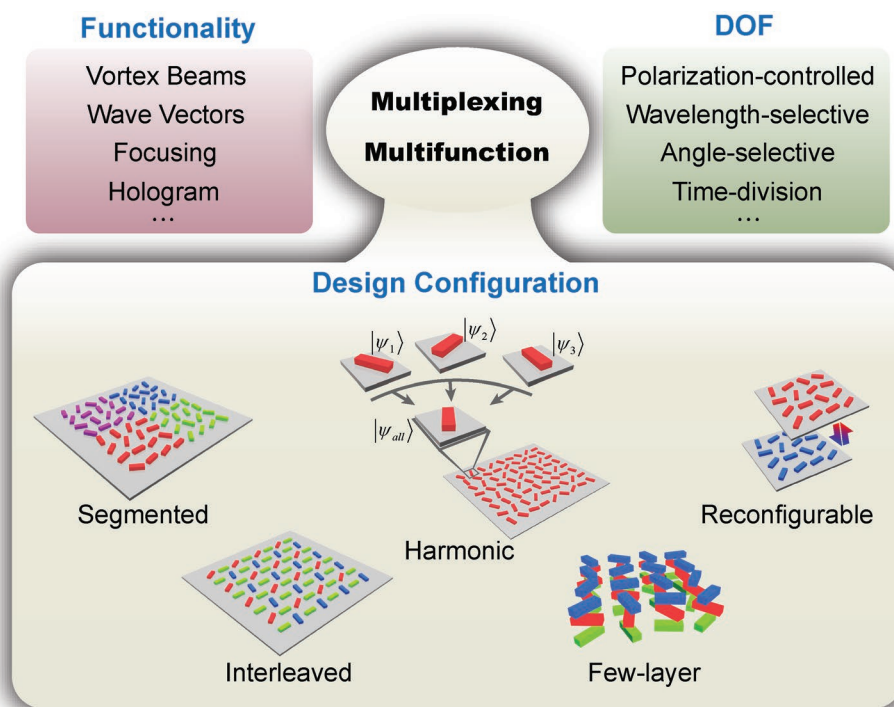


Figure 1. Overview of the development of optical multiplexing and optical multifunctional metasurfaces. Optical multiplexing is generally aimed at optical communication, and optical multifunction is used to deal with concurrent tasks, both of which can integrate different channels or functionalities into a single metasurface. The optical channels consist of vortex beams, wave vectors, holograms, etc., that are manipulated under different wavelengths, incident angles, polarization states, or time series. The configuration of the multiplexing and multifunctional metasurfaces includes segmented, interleaved, harmonic, few-layer, and reconfigurable designs.

Taking intensity of each nanostructure into consideration, Liu et al. proposed an analysis method to estimate the governed area of each nanostructure (Figure 2f), and calculated the functionality function of the scattered field^[57]

$$F(\mathbf{k}) = \sum_i \frac{|t_i|}{\pi} \exp(i\mathbf{k} \cdot \mathbf{r}_i + \phi_i) \prod_{\nu=x,y} \frac{\sin(k_\nu T_{vi}^{MS}/2)}{k_\nu} \quad (2)$$

where T_{vi}^{MS} describes an equivalent size that the nanostructure can govern in the ν direction. This is a more generalized theory which can describe the scattered field of the metasurface more precisely. The red starred line depicts a class of equivalence following $\phi_i + kx_i = \pi$, which means these nanostructures are equivalent to each other in k -space despite their locations and phase (Figure 2g). This analysis method has been utilized to realize a convex-concave double lens, and to demonstrate the stable condition which can guide the design of metasurfaces (Figure 2h). Recently, Jiang et al. proposed an efficient multiplexing millimeter metasurface that can control the transmitted angle, intensity ratio, and topological charges in each channel.^[58] This work studied angular momentum multiplexing and the corresponding properties in detail (Figure 2i,j). The number of multiplexing channels is associated with the noises in each channel. The more the number of channels is, the relative noises in each channel will be. Thus, the total number of multiplexing channels must have an upper limit. Jin et al. proposed a multiplexing metasurface design with 36 channels, which is so far the highest results.^[59] Based on the multiplexing design and

utilizing interleaved arrays, Zhang et al. combined holography and vortex beam generation, and realized four-channel multifunctional metasurfaces with holography and vortex beam both occupying two channels.^[60]

3. Polarization-Controlled Multiplexing and Multifunctional Metasurfaces

As mentioned above, the realization of a specific optical functionality in metasurfaces is always related to the creation of an optical transmission/reflection function with fixed complex amplitude profile in the metasurface plane.^[61–63] Thus, optical multiplexing can be easily achieved by the superposition of different optical transmission/reflection functions in metasurfaces.^[59,64] Meanwhile, metasurfaces with anisotropic optical responses provide another alternative way for the integration of different optical functionalities. With anisotropic metasurfaces, two different optical transmission/reflection functions can be independently designed in the metasurface for two orthogonal linear-polarized waves respectively, which has been widely used for the realization of polarization-controlled multiplexing and multifunctional devices.^[13,37,38,60,65–78] Figure 3a shows a typical example, this anisotropic metasurface consists of birefringent metallic nanoantennas. The phase delay distributions for x - and y -polarized waves in the proposed metasurface can be manipulated independently by rational design of the structure parameters of the metallic nanoantennas, as shown in Figure 3b. This anisotropic

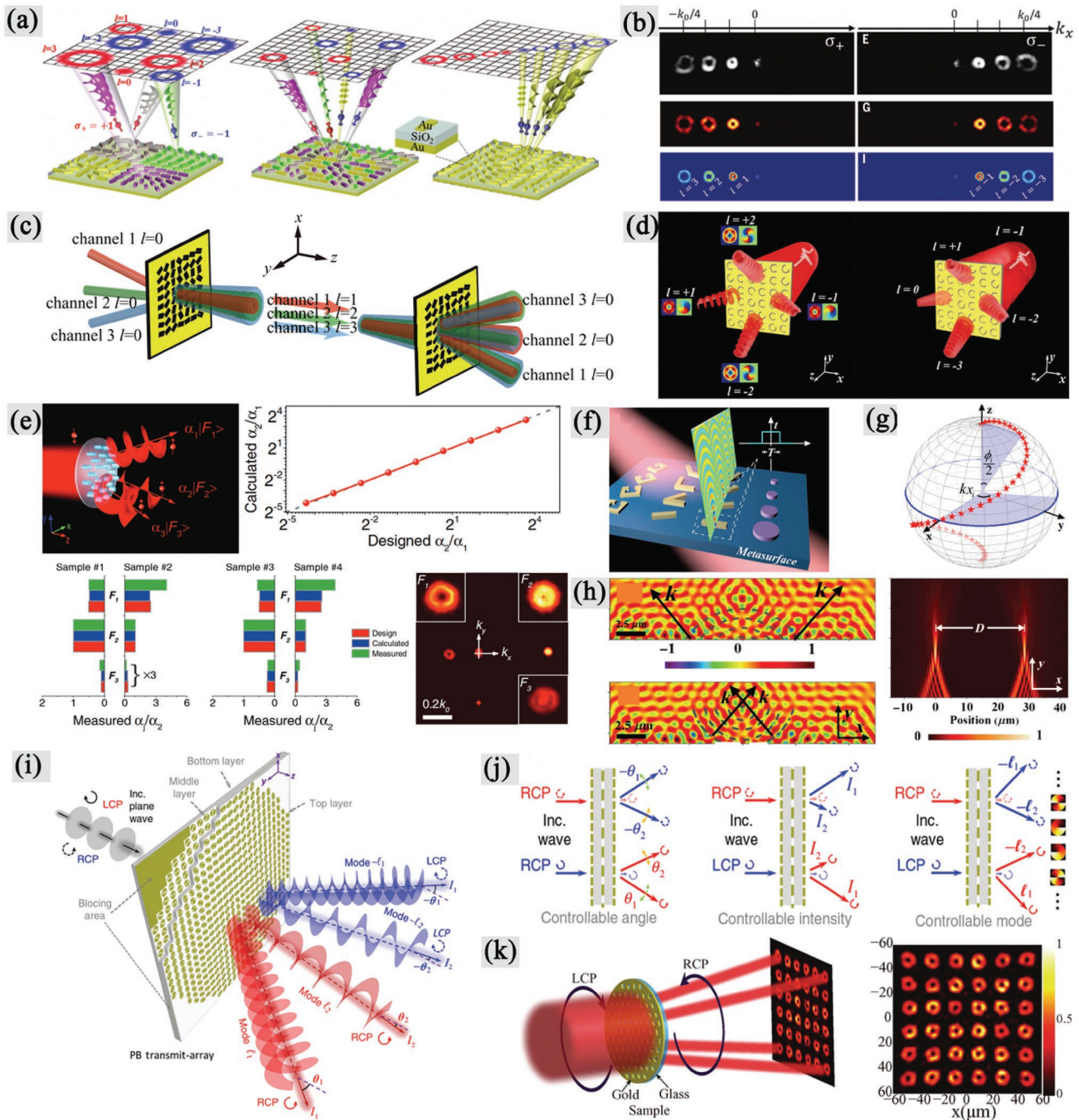


Figure 2. a) Schematic of the shared-aperture metasurfaces that can simultaneously generate vortex beams with different topological charges. b) Top to bottom: measured, simulated, and calculated energy distribution at the Fourier space under left-handed/right-handed circularly polarized (LCP/RCP) incidence, respectively. c) The designed metasurface serves as off-axis multiplexing and demultiplexing for different incident configurations. d) Multiplexing and demultiplexing in the terahertz waveband. e) Energy tailorable multiplexing realized with full Fourier components. By employing both intensity and phase manipulation of the transmitted light with dielectric nanopillars, the intensity of each multiplexing channel can be accurately controlled within a wide design range. f) Localized rectangular model of diffraction theory for multiplexing and multifunctional metasurfaces. Each unit cell has no or weak interaction with other unit cells. g) Sphere of the metaunit. The polar angle is $\phi_i/2$, and the azimuthal angle is kx_i . The red starred line in the sphere is a class of equivalence with $\phi_i + kx_i = \pi$. h) Left to right: designed convex and concave double lens with the momentum analysis method. Periodic focusing with parabolic phase distribution, which is an example of the stable condition. i) Independently controllable intensity, direction, and topological charges of the generation of multiple spin-dependent vortex beams. j) The angles, intensity ratio (I_1/I_2), and topological charges of the output beams can be independently controlled by the metasurfaces. k) A large number of channels generated from the multiplexing metasurfaces. a,b) Reproduced with permission.^[49] Copyright 2016, Wiley-VCH. c) Reproduced with permission.^[54] Copyright 2016, Wiley-VCH. d) Reproduced with permission.^[55] Copyright 2017, American Chemical Society. e) Reproduced with permission.^[56] Copyright 2019, Wiley-VCH. f-h) Reproduced with permission.^[57] Copyright 2017, American Physical Society. i,j) Reproduced with permission.^[58] Copyright 2018, American Physical Society. k) Reproduced with permission.^[59] Copyright 2017, Wiley-VCH.

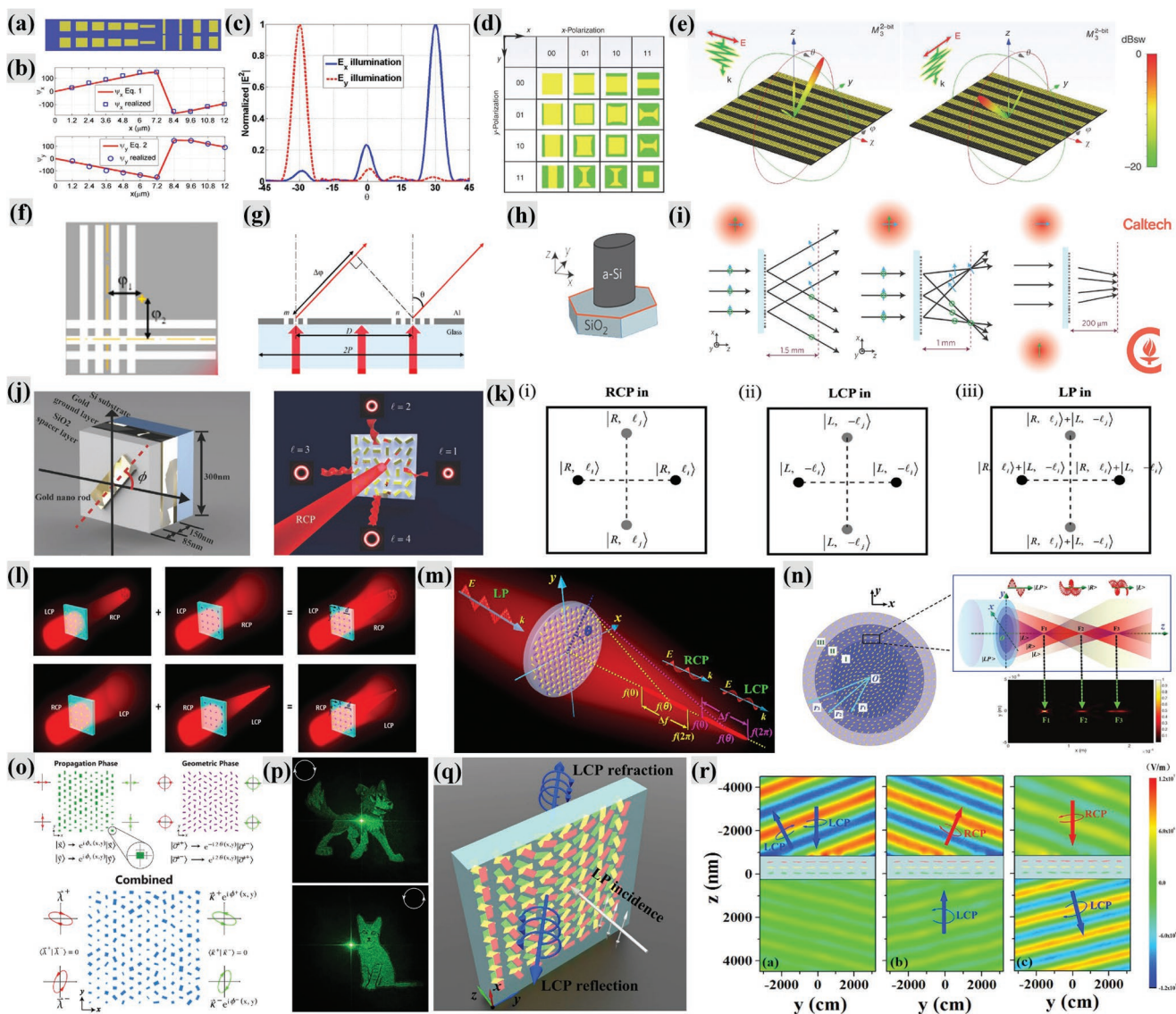


Figure 3. a) Schematic diagram of one period of the metasurface that consists of birefringent nanorods. b) The reflective phase delays of the birefringent nanorods and the corresponding theoretically designed value for x- and y-polarized 8.06 μm optical waves respectively. c) Polarization-controlled anomalous reflection in the designed metasurface. d) Schematic of the basic unit cells of the 2-bit anisotropic coding metasurface. e) Far-field scattering patterns of a 2-bit anisotropic coding metasurface for x- and y-polarized incident waves respectively. f) Schematic of the structural design of the nanoslit-based metasurface for a polarization-controlled hologram. g) Phase and amplitude control of the two typical unit cells in the nanoslit-based metasurface. h) Schematic of an amorphous silicon post, the phase delays of x- and y-polarized waves in the post can be easily manipulated by changing the diameters of the long and short axis of the post respectively. i) Illustration of polarization-controlled beam splitter, focus lens and hologram based on arrays of amorphous silicon post. j) Schematic of a unit cell of the proposed reflective-type metasurface and an artistic rendering of the off-axis multiple orbital angular momentum generation. k) Schematic of the polarization-controlled superpositions of multiple orbital angular momentum for incident waves with different polarization states. l) Schematic of a metasurface with interleaved design for helicity-dependent focusing and holograms. m) Illustration of multifunctional light-sword metasurface lens. n) Schematic of a polarization controlled multifocus metalens with segmented design. o) Conceptual schematic of the combination of propagation and geometric phases, which can be widely used for independent phase manipulation of any set of incident waves with orthogonal polarization states. p) Helicity-dependent hologram at 532 nm. Two independent phase profiles for LCP and RCP waves respectively can be encoded in an array of TiO_2 pillars with the combination of propagation and geometric phases. q) Illustration of the helicity-dependent anomalous wave generation under linearly polarized illumination in a few-layer anisotropic metasurface. r) Electric-field distribution of anomalous waves for LCP and RCP normal incident waves at 1900 nm. a–c) Reproduced with permission.^[65] Copyright 2013, Optical Society of America. d,e) Reproduced with permission.^[66] Copyright 2016, Springer Nature. f,g) Reproduced with permission.^[68] Copyright 2017, American Chemical Society. h,i) Reproduced with permission.^[37] Copyright 2015, Springer Nature. j,k) Reproduced with permission.^[64] Copyright 2017, Wiley-VCH. l) Reproduced with permission.^[71] Copyright 2016, Wiley-VCH. m) Reproduced with permission.^[72] Copyright 2018, American Chemical Society. n) Reproduced with permission.^[75] Copyright 2015, Wiley-VCH. o,p) Reproduced with permission.^[38] Copyright 2017, American Physical Society. q,r) Reproduced under the terms of the CC-BY Creative Commons Attribution 4.0 International License (<http://creativecommons.org/licenses/by/4.0/>).^[13] Copyright 2016, The Authors, published by Springer Nature.

metasurface can deflect x - and y -polarized incident waves into two different directions (Figure 3c), and the deflection angles can be well manipulated independently.^[65] Step further, Liu et al. introduced the concept of coding into the design of anisotropic metasurfaces and realized 1-bit and 2-bit anisotropic coding metasurfaces simultaneously, which provided a simple and effective method for the design of linear-polarization-controlled multifunctional devices.^[66] In the design of 1-bit coding metasurface, two basic unit cells with 0° and 180° phase delay respectively are used as digital element “0” and “1”.^[67] To realize a 2-bit anisotropic coding metasurface, sixteen basic unit cells were used in the proposed design to represent four different digital states, as shown in Figure 3d. With a polarization-dependent coding sequence, the proposed anisotropic coding metasurface can realize distinct optical functionalities for x - and y -polarized incidence (Figure 3e). Figure 3f,g is another typical design of anisotropic metasurface, which is used for the realization of polarization-controlled hologram.^[68] The unit cell of this proposed anisotropic metasurface consists of two sets of nanoslit arrays, the phase and the amplitude of the diffraction waves can be easily manipulated by the detour phase and the number of nanoslits respectively. Moreover, the horizontal arrays and the vertical arrays only diffract vertically polarized waves and horizontally polarized waves respectively. By independently manipulating the phase and amplitude of the x - and y -polarized diffraction waves with the proposed anisotropic metasurface, different holographic images can be observed under different polarization states. The anisotropic optical response exists not only in metallic metasurfaces, but also in dielectric metasurfaces. Figure 3h shows the basic unit cell of a dielectric anisotropic metasurface which is composed of elliptical amorphous silicon posts.^[37] The phase delays of x - and y -polarized waves in the elliptical amorphous silicon post can be directly manipulated by changing the diameters of the long and short axis of the post respectively. By utilizing the elliptical amorphous silicon post, polarization-controlled beam splitters, focus lenses, and holograms have been all well realized with different designs of phase profiles in the metasurface plane (Figure 3i).

In metallic metasurfaces, the phase manipulation of linear-polarized optical waves is associated with its optical resonance.^[69] By adjusting the anisotropic optical resonance in metallic metasurfaces, independent phase manipulation of two orthogonally linear-polarized waves can be easily achieved. Differently, the phase manipulation of circular-polarized optical waves is always realized by using geometric phase, as a result, the phase delays of LCP and RCP optical waves in metallic metasurface always have equal amplitude and opposite sign.^[70] For example, Yue et al. proposed a reflective-type metasurface to realize the generation and polarization-controlled superposition of multiple orbital angular momentum states, as shown in Figure 3j,k.^[64] By switching the polarization state of the incident waves from LCP to RCP, the signs of the topological charges are flipped accordingly. Thus, to realize polarization-controlled multifunctional metasurfaces on the circular base, metasurfaces with interleaved or segmented design have been widely utilized.^[60,71–75] Wen et al. proposed a metasurface with interleaved design to realize two distinct functionalities under LCP and RCP illumination respectively.^[71] The proposed metasurface is a combination

of two different metasurfaces with different optical functionalities, as shown in Figure 3l. For LCP illumination, the RCP wave emitting from the first metasurface reconstructs a holographic image of “cat” while the RCP wave from the second metasurface diverges and forms a subtle background. For RCP illumination, The LCP wave emitting from the second metasurface focus on a spot while the LCP wave from the first metasurface diverges. Thus, this merged metasurface functions as a hologram and a convex lens for LCP and RCP illumination respectively. By using the same design principle, Zhang et al. realized a light sword metasurface lens with helicity-dependent focal segment, as shown in Figure 3m.^[72] Figure 3n shows a helicity-dependent multifoci metalens based on the segmented design.^[75] The proposed metalens is comprised of three regions with different phase profiles. Every region can be considered as a helicity-dependent sublens and these three sublenses have the same axis and different focal lengths. Thus, the proposed metasurface can focus LCP and RCP illumination into different spots. Even though polarization-controlled multifunctional metasurfaces on the circular base can be easily realized by using interleaved and segmented design in metasurfaces, the unit cell of these designs cannot realize independent phase manipulation of LCP and RCP optical waves, resulting in the reduction of the working efficiency of metasurfaces and introducing extra background noises. Based on the previous approach,^[37] Mueller et al. presented an effective method to overcome these disadvantages and realized the independent phase manipulation of any pair of orthogonal states of polarization in one dielectric pillar.^[38] Figure 3o is a conceptual schematic of the proposed method, and independent phase profiles on any set of orthogonal polarization states can be realized in dielectric nanostructure arrays by combining the geometric and propagation phases. With this approach, chiral holograms were realized in dielectric metasurfaces composed of TiO_2 pillars, as shown in Figure 3p. Another alternative approach to realize full and dispersionless phase and polarization control of optical waves is to involve diatomic metamolecules that are composed of two orthogonal meta-atoms.^[39] By tailoring the global and local displacements between and within each metamolecules, fully and independent manipulation of phase and polarization of optical waves can be realized. Based on this approach, broadband vectorial metahologram has been well implemented. Recently, Li et al. extended a new degree of freedom for the design of polarization-controlled multifunctional devices.^[13] With simultaneous manipulation of phase and amplitude of optical waves, the anomalous wave generation in the proposed few-layer metasurface not only depends on the helicity of the incident waves but also is relate to the incident directions, as shown in Figure 3q,r. With this approach, a series of new polarization-controlled multifunctional devices have continually been proposing.^[76–78] It is worth mentioning that polarization-controlled multifunctional metasurfaces not only can be realized by involving effective phase manipulation of optical waves in metasurfaces, but also can be realized by involving effective intensity manipulation of optical waves in metasurfaces. For example, Li et al. proposed a bilayer aluminum metasurface to realize the arbitrary intensity manipulation of optical waves.^[79] Polarization-controlled imaging and optical

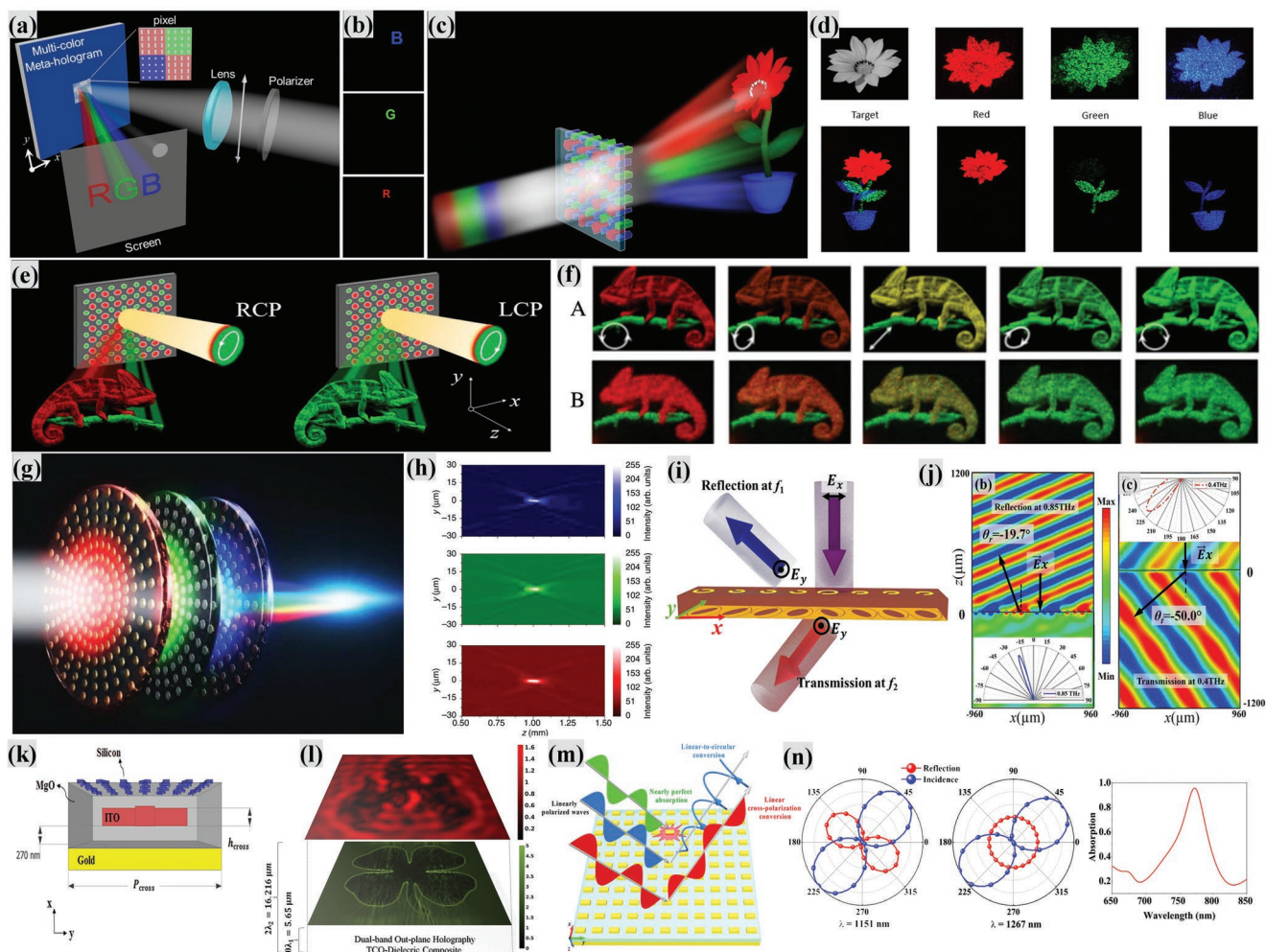


Figure 4. a) Illustration of a multicolor hologram under linearly polarized incidence in an aluminum-nanorod-based array. b) The locations and sizes of the three wavelength-selective images relative to the zeroth-order spot. c) Illustration of multiwavelength hologram in a dielectric interleaved array. d) Experimental measured results of the achromatic color hologram (top half) and highly dispersive color hologram (bottom half). e) Schematic of the polarization-controlled color hologram in a dielectric interleaved metasurface. f) Target holographic images for different polarization states (A), and the corresponding experimental measured results (B), while lasers of 632.8 and 532 nm provide illumination simultaneously. g) Schematic of multispectral achromatic lens based on a few-layer design. h) Experimentally measured results of focal spot for the few-layer metasurface at 450, 550, and 650 nm, showing the chromatic aberration correction. i) Illustration of the bifunctional beam deflector. j) Electric-field distributions of y -polarized component and the far-field responses at 0.85 THz (reflection) and 0.4 THz (transmission) for the x -polarized normal incidence. k) Schematic of the few-layer metasurface for multispectral holograms. l) Calculated results of dual-wavelength out-of-plane holographic images. m) Illustration of the multifunctional metasurface. n) Simulated results of linear cross-polarization conversion, linear-to-circular conversion and nearly perfect absorption in three different wavelengths. a, b) Reproduced with permission.^[80] Copyright 2015, American Chemical Society. c, d) Reproduced with permission.^[81] Copyright 2016, American Chemical Society. e, f) Reproduced with permission.^[82] Copyright 2017, Optical Society of America. g, h) Reproduced under the terms of the CC-BY Creative Commons Attribution 4.0 International License (<http://creativecommons.org/licenses/by/4.0/>).^[83] Copyright 2017, The Authors, published by Springer Nature. i, j) Reproduced under the terms of the CC-BY Creative Commons Attribution 4.0 International License (<http://creativecommons.org/licenses/by/4.0/>).^[84] Copyright 2018, The Authors, published by Springer Nature. k, l) Reproduced with permission.^[87] Copyright 2018, American Chemical Society. m, n) Reproduced with permission.^[88] Copyright 2017, AIP Publishing.

encryption have been well demonstrated by utilizing the proposed bilayer metasurface.

4. Wavelength-Selective Multiplexing and Multifunctional Metasurfaces

Realizing specific optical functionalities at different wavelengths is a fundamental requirement of the development of

the integrated photonics, which requires independent design of the optical transmission/reflection functions of the optical devices at different wavelengths. Metasurfaces with interleaved, segmented or few-layer design provide an effective way for the realization of wavelength-selective multiplexing and multifunctional devices.^[80–87] For example, Huang et al. utilized an interleaved aluminum nanorod array to realize a phase-modulated multicolor meta-hologram for linearly polarized illumination, as shown in **Figure 4a,b**.^[80] The unit

cell of the proposed metasurface consists of four subunits that can realize independent phase manipulation of optical waves at three different wavelengths, while keeping the same efficiency. With this approach, three different phase profiles corresponding to different holographic images were simultaneously achieved in the metasurface plane, resulting in the multicolor meta-hologram. By utilizing the same design concept, Wang et al. proposed a dielectric metasurface composed of Si nanoblocks to realize independent and full phase control at red, green and blue wavelengths for circular-polarized illumination.^[81] They further achieved achromatic color hologram and highly dispersive color hologram to verify the successful phase manipulation at three visible wavelengths, as shown in Figure 4c,d. Polarization-controlled color-tunable holograms can even be achieved in interleaved metasurfaces by utilizing both polarization-controlled and wavelength-selective manipulation of optical waves.^[82] As shown in Figure 4e, the unit cell of the proposed metasurface consists of two Si nanopillars, and each of them was used to construct a specific phase profile at a fixed wavelength for a certain polarization state. By using this design concept, twin holographic images of a “chameleon” were achieved for LCP green illumination and RCP red illumination. Due to color mixing, the color of the holographic image of the “chameleon” can be easily tuned by changing the polarization state of the incident waves, as shown in Figure 4f. Different from interleaved or segmented metasurfaces, the realization of the wavelength-selective multifunctionalities in few-layer metasurfaces is attributed to the layer-by-layer design of the optical transmission/reflection functions for different wavelengths. For example, Avayu et al. utilized a metallic few-layer metasurface to realize a triply (red, green, and blue) achromatic metalens, as shown in Figure 4g,h.^[83] The proposed few-layer metasurface is a vertical stacking of three independent metasurfaces, and every of them is made from a different material and is designed for a fixed wavelength. Figure 4i shows another few-layer design that is composed of two independent metasurfaces.^[84] This design was utilized to generate anomalous refraction and reflection at two different wavelengths respectively, as shown in Figure 4j. Wavelength-selective bi-functional deflectors and bi-functional focusing lenses were also achieved by this design. Since the optical transmission/reflection functions for two wavelengths can be independently designed in two layers, the optical functionality of this type of two-layer design at each wavelength can be arbitrarily designed.^[85,86] For metasurfaces with few-layer design, it is worth mentioning that the size of the unit cell of each layer do not need to be the same, Figure 4k is a typical example.^[87] The proposed few-layer metasurface is also composed of two independent metasurfaces; the top layer consists of Si nanorods and the bottom layer is composed of ITO cross-shaped nanoantennas. Because the size of the unit cell of the bottom layer is much bigger than the top layer, the optical functionality at two wavelengths that are far apart can be independently designed. With the proposed few-layer metasurface, dual-wavelength out-of-plane hologram at the operating frequencies of 531 and 37 THz were achieved, as shown in Figure 4l. This approach indicates that few-layer metasurfaces have advantages in the design of wavelength-selective multifunctional devices when the desired operating wavelengths are far apart. Different from the above design concepts,

Cheng et al. utilized an array of gold nanorods to realize linear cross-polarization conversion, linear-to-circular conversion, and nearly perfect absorption in three different wavelengths respectively, as shown in Figure 4m,n.^[88] The realization of wavelength-selective multifunctionalities in the proposed design is attributed to the reasonable optimization of the anisotropic resonance of the nanorod in a broadband range. Even though the proposed metasurface has a good performance, the huge time for structure optimization makes this design concept cannot be widely used for the design of wavelength-selective multifunctional devices. However, the development of artificial intelligence provides a new opportunity for the application of the proposed design concept.^[89] With significant decrease of the time for structure optimization, the proposed design concept may become an effective way for the design of wavelength-selective multifunctional devices in future. Moreover, recent advances in nonlinear metasurfaces provide a new approach for the realization of wavelength-selective multiplexing and multifunctional metasurfaces.^[90,91] Nonlinear metasurfaces, which can realize phase manipulation of fundamental optical waves and harmonic waves simultaneously, can implement different optical functionalities at fundamental wavelengths and harmonic wavelengths respectively. Predictably, nonlinear metasurfaces will be an important part of the research area of multiplexing and multifunctional metasurfaces.

5. Angle-Selective Multiplexing and Multifunctional Metasurfaces

The polarization-controlled or the wavelength-selective multiplexing and multifunctional metasurfaces mentioned above can only realize different optical functionalities by changing the polarization state or the wavelength of the illumination. In some cases, people are more willing to achieve different functionalities in one optical device without changing the state of the illumination, which requires the realization of switchable optical function in optical devices. Angle-selective metasurfaces provide an effective way to meet this need. For example, Kamali et al. proposed an angle-multiplexed metasurfaces to realize independent wave-front encoding at different illumination angles.^[92] The proposed metasurface composed of dielectric U-shaped nanostructures shows different optical responses at different illumination angles, resulting in the realization of incident-angle-selective phase profile in the metasurface plane. Based on this design concept, angle-multiplexed hologram was achieved. Two different holographic images can be observed under 0° and 30° illumination respectively, as shown in Figure 5a,b. Angle-selective multifunctional metasurfaces have also been proposed to effectively realize the manipulation of optical wave front. Deng et al. showed that extraordinary optical transmission, total internal reflection and extraordinary optical diffraction could be realized respectively in a metallic nanoslit array that is embedded in an asymmetric environment for three different illumination angles.^[93] This multifunctional metasurface can be treated as a transmission filter, a mirror, and an off-axis lens simultaneously. Polarization manipulation of optical waves can also be implemented in angle-selective metasurfaces. Figure 5c,d shows an angle-selective multifunctional device that

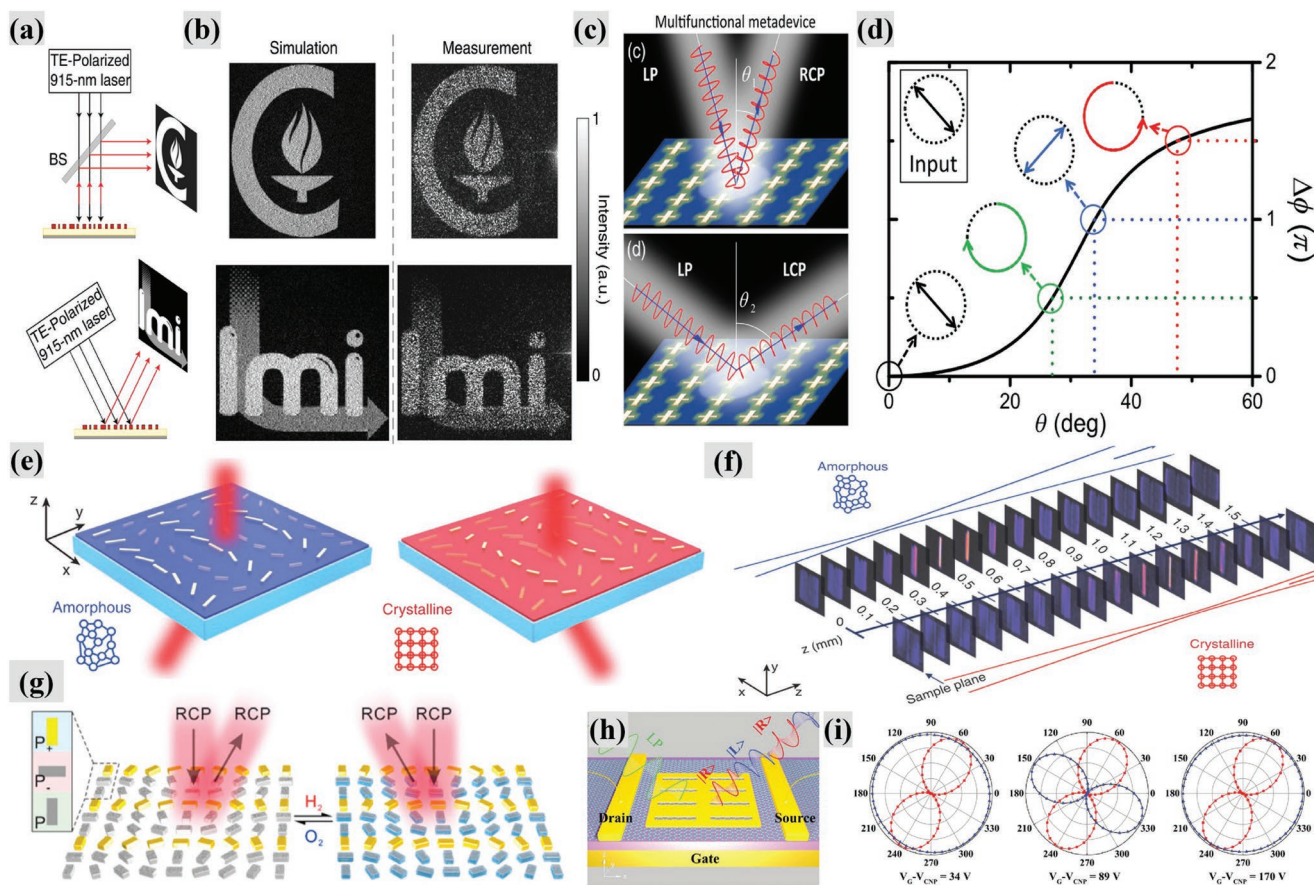


Figure 5. a) Illustration of the angle-multiplexed hologram. b) Simulated and experimental measured holographic images captured under a 915 nm TE-polarized laser at 0° and 30° incidence angles. c) Schematics of an incidence-angle-dependent multifunctional metasurface for polarization manipulation of reflected waves. d) Calculated results of TE-TM reflection-phase difference at different illumination angles at 0.55 THz. e) Illustration of beam switching in the active plasmonic metasurface. f) Camera pictures of the bifocal lens imaged at different distances z from the metasurface. g) Illustration of tunable beam steering in a dynamic Janus metasurface. h) Schematic of a graphene-loaded plasmonic metasurface for optical polarization encoding. i) Simulated polarization states of incident (red) and reflected (blue) light at $7.1 \mu\text{m}$ for different gate voltages. a,b) Reproduced with permission.^[92] Copyright 2017, American Physical Society. c,d) Reproduced with permission.^[94] Copyright 2018, American Physical Society. e,f) Reproduced with permission.^[99] Copyright 2017, Springer Nature. g) Reproduced with permission.^[100] Copyright 2018, American Chemical Society. h,i) Reproduced with permission. Copyright 2015, Wiley-VCH.^[105]

can behave as a half- or a quarter-wave plate under different illumination angles.^[94] Recent advances in angle-selective multifunctional metasurfaces further indicate that the optical response of metasurfaces with interleaved design can be simultaneously and independently manipulated by the wavelength, the polarization and the incident angle of optical waves, which greatly expand the design range of multifunctional metasurfaces.^[95] The introduction of incident-angle-selective optical responses in metasurfaces provides a new DOF for the design of multifunctional optical devices and significantly expands the practical applications of metasurfaces.

6. Reconfigurable Metasurfaces for Time Division Multiplexing

Reconfigurable metasurfaces can also be used for the realization of multiplexing and multifunctional optical devices for a fixed illumination. Recently, reconfigurable metasurfaces made

from phase change materials, liquid metals, graphene and so on have been widely investigated to realize the dynamic manipulation of optical waves.^[96–104] Figure 5e shows a reconfigurable metasurface for dynamic tunable beam switching.^[99] The proposed design is composed of a GeSbTe (GST) layer and a geometric phase metasurface. The geometric phase metasurface based on interleaved design can realize two specific phase profiles at two resonant peaks. GST is a typical phase change material. When the phase of the GST changed from amorphous to crystalline, the resonance peaks of the geometric phase metasurface will red-shift accordingly. Thus, for a fixed incident wavelength, the phase profile in the metasurface plane can be switched between two designed states by changing the phase of the GST, resulting in the dynamically tunable beam switching. With this design concept, bifocal zoom lens were further achieved, as shown in Figure 5f. Yu et al. utilized another reconfigurable metasurface composed of gold and magnesium nanorods to realize dynamic multifunctional devices in the visible spectral region.^[100] Magnesium can undergo a

phase-transition from metal to dielectric upon hydrogen. With hydrogenation and dehydrogenation process, the phase profile in the proposed metasurface plane can be switched between two states, resulting in two different optical responses for a fixed illumination, as shown in Figure 5g. Above approaches indicate that reconfigurable metasurfaces made from phase change materials can be widely used for the realization of the dynamic bifunctional devices. However, metasurfaces made from phase change materials have some disadvantages on the realization of dynamic trifunctional or multifunctional devices, because it can only switch the optical transmission function of the metasurfaces between two designed states. Recently, metasurfaces made from graphene show some advantages on the realization of dynamic multifunctional devices. The optical conductivity and permittivity of graphene show a strong dependence on its Fermi level, which can be dynamically controlled by a gate voltage.^[102–105] By combining the graphene layer with an anisotropic gold nanoaperture array, Li et al. realized dynamic and continuous modulation of the polarization states of the reflected waves.^[105] The polarization state of the reflected waves can be dynamically manipulated into linear-polarized, LCP and RCP by changing the gate voltage among three different values, as shown in Figure 5h,i. As a dynamic approach for the implementation of optical multiplexing and multifunction integration, reconfigurable metasurfaces plays a key role in the research area of multiplexing and multifunctional metasurfaces and is attracting more and more attention of the scientific community.

7. Integrated and On-Chip Multifunctional Metasurfaces

Although the compact size is one of the most intriguing properties of metasurfaces, we usually have to handle them and measure their optical properties with huge equipment. In the past decades, researchers were studying on developing integrated and on-chip metamaterials and metasurfaces, which combines sources, processor, and detectors all together, so that they can be as successful as electronic industry one day. However, integrated design is challenging due to the theoretical design principle, fabrication techniques, and compatibility of each subcomponent. In the metasurfaces platform, researchers are still seeking for valuable scenarios from different point of views to realize integrated and on-chip techniques. Zhang et al. proposed a design of geometric dielectric metasurface that locates on top of a traditional waveguide. Interestingly, for different incident polarization states, the light that couples into the waveguide can be selectively transmitted, which is attributed to the coupling between the waveguide modes and the surface waves generated by the metasurface (Figure 6a,b).^[106] Li et al. combined a waveguide and phase-gradient metasurfaces to control the propagation and coupling of waveguide modes.^[107] The nanostructures lay on top of the waveguide. For forward propagation direction, the incident fundamental waveguide mode TE_{00} is converted either to higher-order TE or TM modes; while for backward propagation direction, the incident fundamental waveguide mode is converted to surface waves (Figure 6c). As shown in Figure 6d, the forward incident TE_{00} mode is

converted to TM_{00} mode. Such mode conversion as special type waveguide may find applications in high-capacity optical communication. Integrated metalens develops rapidly recently since doublet lens can be utilized to eliminate chromatic aberrations.^[108,109] As shown in Figure 6e, Arbabi et al. employed a doublet metalens integrated with a complementary metal-oxide-semiconductor (CMOS) detector, and achieved a minimized camera with total size of $1.6 \text{ mm} \times 1.6 \text{ mm} \times 1.7 \text{ mm}$.^[109] The proposed minimized camera not only can correct chromatic aberrations with field-of-view of 60° , but also can record images directly. Li et al. realized on-chip zero-index nanostructures design,^[110] which is integrated with conventional photonic components such as SU-8 slab waveguide, and can be efficiently coupled to photonic integrated circuits and other optical components (Figure 6f,g). Actually, the scale of metasurfaces decides that they are much easier to be integrated than traditional optical elements. Wang et al. proposed a compact design to generate high-order Laguerre–Gaussian modes with a plasmonic metasurface (Figure 6h).^[111] With delicate design of pixel distribution, Shen et al. realized polarization-selective waveguide mode splitter with total size of $2.4 \mu\text{m} \times 2.4 \mu\text{m}$.^[112] As shown in Figure 6i, different polarized waveguide modes (TE and TM modes) propagate to different branches. Such dielectric building blocks are compatible with CMOS fabrication processes, which is considered to be a candidate for future integrated photonic systems.^[113–115] Recently, Arbabi et al. proposed tunable metasurface doublets based on microelectromechanical systems (MEMS),^[116] which theoretically enables a scanning frequency reaching a few kHz (Figure 6j). By controlling the relative distance between two metalenses, the focal spot alters for about $35 \mu\text{m}$. The proposed design can also be integrated with a third metasurface to form a minimized microscope, and the corrected field-of-view reaches 40° .

8. Conclusions and Outlook

Here, we have presented the development of multiplexing and multifunctional metasurfaces. With elaborate design of nanostructure arrays, different information can be multiplexed into different channels, or different functionalities can be integrated. The functionalities are not limited to vortex beams, others such as focusing, imaging, holography, surface waves, waveguide modes conversion, special beams, can also be used as functionality channels. Since metasurfaces provide a wide platform for deep light-matter interaction and for manipulating different optical dimensions, metasurfaces can deal with concurrent tasks at different polarizations, wavelengths, and incident angles, which further greatly boosts the DOF to realize multifunctional designs. By controlling unit cells through optical, mechanical and many other methods, reconfigurable multifunctional metasurfaces enable functionalities to transform to another ones, which significantly reduces the costs of fabrications. On the other hand, metasurfaces, especially all-dielectric metasurfaces, are compatible with the commercial CMOS platform,^[117] and can potentially combine existing photonic elements such as waveguides, quantum dots. Consequently, integrated and on-chip metasurfaces that can perform optical communication and optical computation may also be

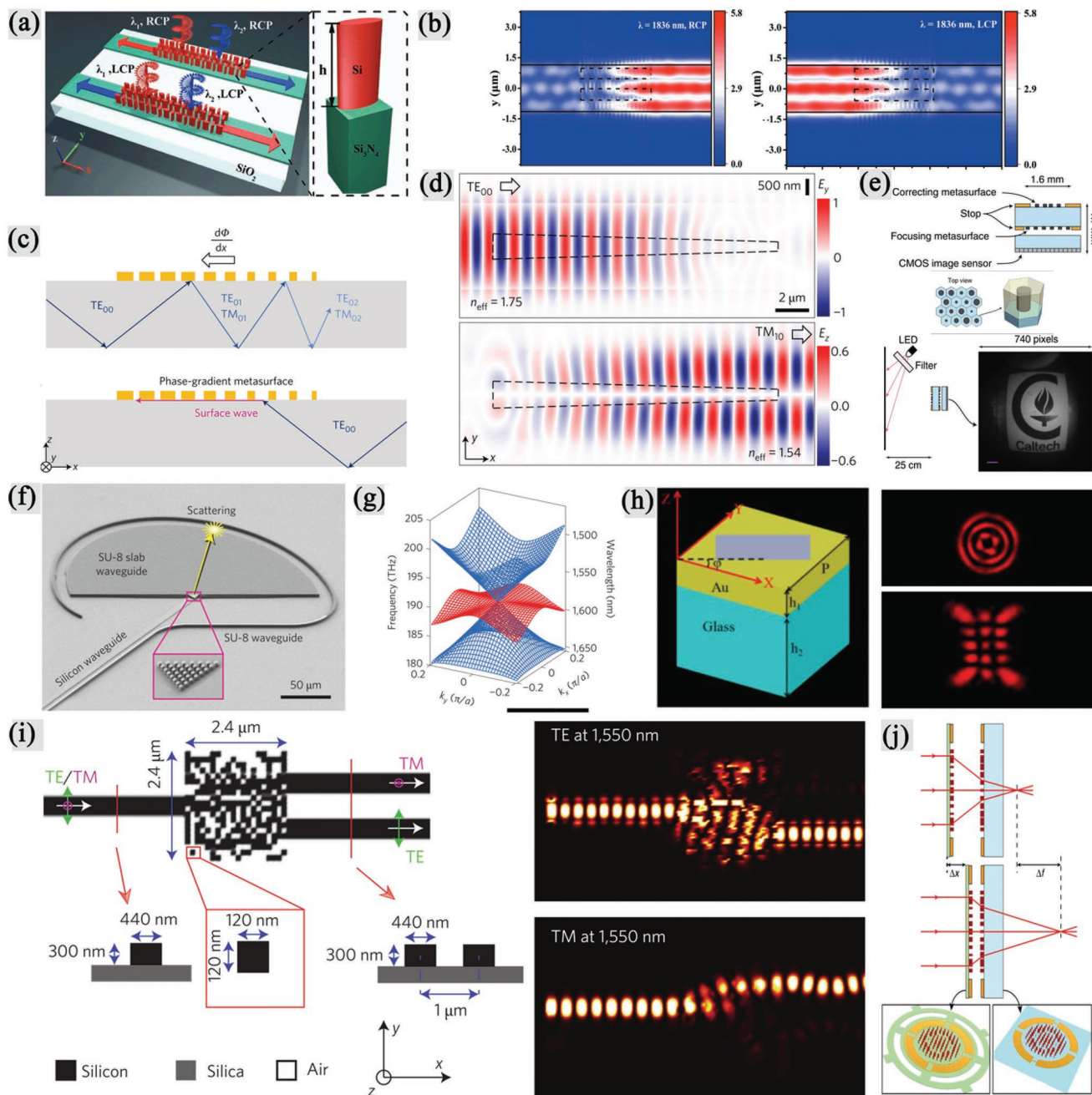


Figure 6. a) Under circularly polarized incidence, the metasurface-waveguide generated spin-selective surface waves that are guided to two opposite directions. b) Left to right: simulated output electric distribution for RCP and LCP incidence. c) Top to bottom: with forward propagation direction, the incidence fundamental waveguide mode is transferred to either higher-order TE or TM modes; whereas with backward propagation direction, the incident fundamental waveguide mode is transferred into surface waves. d) Mode transfer from TE₀₀ to TM₁₀ when light propagates along the waveguide. e) Integrated miniature camera that can correct chromatic aberrations and imaging simultaneously, with total size of 1.6 mm × 1.6 mm × 1.7 mm. f) On-chip zero-index metasurfaces, which is integrated with conventional nanophotonic components such as an SU-8 slab waveguide. g) 3D dispersion surfaces of the zero-index metasurface. h) On-chip generation of high-order Laguerre–Gaussian modes with broadband metasurfaces. i) Integrated beam splitter that can separate the TE and TM output beam into two paths. j) An integrated MEMS-tunable metalens. The focal length is dynamically tuned by controlling the distance between two metalenses using a MEMS system. a,b) Reproduced with permission.^[106] Copyright 2019, Wiley-VCH. c,d) Reproduced with permission.^[107] Copyright 2017, Springer Nature. e) Reproduced under the terms of the CC-BY Creative Commons Attribution 4.0 International License (<http://creativecommons.org/licenses/by/4.0/>).^[109] Copyright 2016, The Authors, published by Springer Nature. f,g) Reproduced with permission.^[110] Copyright 2015, Springer Nature. h) Reproduced with permission.^[111] Copyright 2017, Optical Society of America. i) Reproduced with permission.^[112] Copyright 2015, Springer Nature. j) Reproduced under the terms of the CC-BY Creative Commons Attribution 4.0 International License (<http://creativecommons.org/licenses/by/4.0/>).^[116] Copyright 2018, The Authors, published by Springer Nature.

possible. As mentioned above, integrated and on-chip design of metasurfaces mainly suffer from the lack of multidimensional manipulation of optical waves, the lack of universal design strategy, limited fabrication techniques, and increased signal to noise ratio. One way to overcome such limitations may be developing new materials to improve the intrinsic properties of metasurfaces, such as 2D photonic materials. Another way may be exploiting new DOF to manipulate optical fields. Recently, the burgeoning development of photonic and phononic topology is a good example,^[118,119] which roots in the intrinsic symmetries of materials or structures to manipulate the energy band. As the development of deep subwavelength nanostructures, multiplexing and multifunctional metasurfaces will have deeper and deeper impact on modern photonics, quantum optics, and relative techniques.

Acknowledgements

This work was supported by the National Key Research and Development Program of China (2016YFA0301102 and 2017YFA0303800), the National Natural Science Foundation of China (11974193, 91856101, 11774186, and 11574163), the Natural Science Foundation of Tianjin for Distinguished Young Scientists (18JCQJC45700), the China Postdoctoral Science Foundation (2018M640224 and 2018M640229), the Natural Science Foundation of Tianjin (16JCQNJC01700), and the 111 Project (B07013).

Conflict of Interest

The authors declare no conflict of interest.

Keywords

flat optical elements, integrated photonic devices, metasurfaces, multifunction, multiplexing

Received: September 12, 2018

Revised: July 3, 2019

Published online: October 16, 2019

- [1] N. Yu, P. Genevet, M. A. Kats, F. Aieta, J. P. Tetienne, F. Capasso, Z. Gaburro, *Science* **2011**, 334, 333.
- [2] N. Meinzer, W. L. Barnes, I. R. Hooper, *Nat. Photonics* **2014**, 8, 889.
- [3] S. Larouche, D. R. Smith, *Opt. Lett.* **2012**, 37, 2391.
- [4] H. T. Chen, A. J. Taylor, N. Yu, *Rep. Prog. Phys.* **2016**, 79, 076401.
- [5] Z. Liu, Z. Li, Z. Liu, J. Li, H. Cheng, P. Yu, W. Liu, C. Tang, C. Gu, J. Li, S. Chen, J. Tian, *Adv. Funct. Mater.* **2015**, 25, 5428.
- [6] P. Yu, J. Li, C. Tang, H. Cheng, Z. Liu, Z. Li, Z. Liu, C. Gu, J. Li, S. Chen, J. Tian, *Light: Sci. Appl.* **2016**, 5, e16096.
- [7] J. Q. Li, N. Verellen, P. Dorpe, *ACS Photonics* **2017**, 4, 1893.
- [8] Z. Liu, S. Du, A. Cui, Z. Li, Y. Fan, S. Chen, W. Li, J. Li, C. Gu, *Adv. Mater.* **2017**, 29, 1606298.
- [9] J. Tian, H. Luo, Q. Li, X. Pei, K. Du, M. Qiu, *Laser Photonics Rev.* **2018**, 12, 1800076.
- [10] S. Chen, H. Cheng, H. Yang, J. Li, X. Duan, C. Gu, J. Tian, *Appl. Phys. Lett.* **2011**, 99, 253104.
- [11] W. Yue, S. Gao, S.-S. Lee, E.-S. Kim, D.-Y. Choi, *Laser Photonics Rev.* **2017**, 11, 1600285.
- [12] A. Tittl, A. Leitis, M. Liu, F. Yesilkoy, D. Y. Choi, D. N. Neshev, Y. S. Kivshar, H. Altug, *Science* **2018**, 360, 1105.
- [13] Z. Li, W. Liu, H. Cheng, J. Liu, S. Chen, J. Tian, *Sci. Rep.* **2016**, 6, 35485.
- [14] C. Menzel, C. Helgert, C. Rockstuhl, E. B. Kley, A. Tunnermann, T. Pertsch, F. Lederer, *Phys. Rev. Lett.* **2010**, 104, 253902.
- [15] E. Rahimi, R. Gordon, *Adv. Opt. Mater.* **2018**, 6, 1800274.
- [16] Y. Shen, V. Rinnerbauer, I. Wang, V. Stelmakh, J. D. Joannopoulos, M. Soljačić, *ACS Photonics* **2015**, 2, 27.
- [17] Y. Yang, W. Wang, A. Boulesbaa, I. I. Kravchenko, D. P. Briggs, A. Poretzky, D. Geohegan, J. Valentine, *Nano Lett.* **2015**, 15, 7388.
- [18] Y. Zhang, W. Liu, Z. Li, Z. Li, H. Cheng, S. Chen, J. Tian, *Opt. Lett.* **2018**, 43, 1842.
- [19] G. Borrmann, *Z. Phys.* **1950**, 127, 297.
- [20] L. Huang, X. Chen, H. Mühlenbernd, G. Li, B. Bai, Q. Tan, G. Jin, T. Zentgraf, S. Zhang, *Nano Lett.* **2012**, 12, 5750.
- [21] A. A. Mohammadreza Khorasaninejad, P. Kanhaiya, F. Capasso, *Sci. Adv.* **2016**, 2, e1501258.
- [22] W. Liu, Z. Li, H. Cheng, C. Tang, J. Li, S. Zhang, S. Chen, J. Tian, *Adv. Mater.* **2018**, 30, 1706368.
- [23] J. Lin, P. Genevet, M. A. Kats, N. Antoniou, F. Capasso, *Nano Lett.* **2013**, 13, 4269.
- [24] Z. -L. Deng, S. Zhang, G. Wang, *Nanoscale* **2016**, 8, 1588.
- [25] M. Khorasaninejad, A. Ambrosio, P. Kanhaiya, F. Capasso, *Sci. Adv.* **2016**, 2, e1501258.
- [26] Z. -L. Deng, S. Zhang, G. P. Wang, *Opt. Express* **2016**, 24, 23118.
- [27] C. Min, J. Liu, T. Lei, G. Si, Z. Xie, J. Lin, L. Du, X. Yuan, *Laser Photonics Rev.* **2016**, 10, 978.
- [28] G. Li, S. Chen, N. Pholchai, B. Reineke, P. W. Wong, E. Y. Pun, K. W. Cheah, T. Zentgraf, S. Zhang, *Nat. Mater.* **2015**, 14, 607.
- [29] Z. -L. Deng, J. Deng, X. Zhuang, S. Wang, T. Shi, G. P. Wang, Y. Wang, J. Xu, Y. Cao, X. Wang, X. Cheng, G. Li, X. Li, *Light: Sci. Appl.* **2018**, 7, 78.
- [30] S. Wu, Z. Zhang, Y. Zhang, K. Zhang, L. Zhou, X. Zhang, Y. Zhu, *Phys. Rev. Lett.* **2013**, 110, 207401.
- [31] W. Liu, S. Chen, Z. Li, H. Cheng, P. Yu, J. Li, J. Tian, *Opt. Lett.* **2015**, 40, 3185.
- [32] Z. Li, W. Liu, H. Cheng, S. Chen, J. Tian, *Sci. Rep.* **2016**, 5, 18106.
- [33] P. Yu, S. Chen, J. Li, H. Cheng, Z. Li, W. Liu, B. Xie, Z. Liu, J. Tian, *Opt. Lett.* **2015**, 40, 3229.
- [34] Z. Li, H. Cheng, Z. Liu, S. Chen, J. Tian, *Adv. Opt. Mater.* **2016**, 4, 1230.
- [35] J. Li, S. Chen, H. Yang, J. Li, P. Yu, H. Cheng, C. Gu, H. -T. Chen, J. Tian, *Adv. Funct. Mater.* **2015**, 25, 704.
- [36] L. Liu, X. Zhang, M. Kenney, X. Su, N. Xu, C. Ouyang, Y. Shi, J. Han, W. Zhang, S. Zhang, *Adv. Mater.* **2014**, 26, 5031.
- [37] A. Arbabi, Y. Horie, M. Bagheri, A. Faraon, *Nat. Nanotechnol.* **2015**, 10, 937.
- [38] J. P. Balthasar Mueller, N. A. Rubin, R. C. Devlin, B. Groever, F. Capasso, *Phys. Rev. Lett.* **2017**, 118, 113901.
- [39] Z. -L. Deng, J. Deng, X. Zhuang, S. Wang, K. Li, Y. Wang, Y. Chi, X. Ye, J. Xu, G. P. Wang, R. Zhao, X. Wang, Y. Cao, X. Cheng, G. Li, X. Li, *Nano Lett.* **2018**, 18, 2885.
- [40] W. Chen, M. Khorasaninejad, R. C. Devlin, J. Oh, A. Y. Zhu, F. Capasso, *Science* **2016**, 352, 1565.
- [41] C. Schlickriede, N. Waterman, B. Reineke, P. Georgi, G. Li, S. Zhang, T. Zentgraf, *Adv. Mater.* **2018**, 30, 1703843.
- [42] M. Khorasaninejad, F. Capasso, *Science* **2017**, 358, eaam8100.
- [43] X. Zhang, F. Dong, F. Yue, C. Zhang, L. Xu, Z. Song, M. Chen, P. Y. Chen, G. S. Buller, Y. Zhu, S. Zhuang, W. Chu, S. Zhang, X. Chen, *Adv. Mater.* **2018**, 30, 1707499.
- [44] Q. Wei, L. Huang, X. Li, J. Liu, Y. Wang, *Adv. Opt. Mater.* **2017**, 5, 1700434.

- [45] Z. -L. Deng, G. Li, *Mater. Today Phys.* **2017**, *3*, 16.
- [46] A. B. Khanikaev, N. Arju, Z. Fan, D. Purtseladze, F. Lu, J. Lee, P. Sarriguarte, M. Schnell, R. Hillenbrand, M. A. Belkin, G. Shvets, *Nat. Commun.* **2016**, *7*, 12045.
- [47] D. C. Hooper, A. G. Mark, C. Kuppe, J. T. Collins, P. Fischer, V. K. Valev, *Adv. Mater.* **2017**, *29*, 1605110.
- [48] A. E. Willner, H. Huang, Y. Yan, Y. Ren, N. Ahmed, G. Xie, C. Bao, L. Li, Y. Cao, Z. Zhao, J. Wang, M. P. J. Lavery, M. Tur, S. Ramachandran, A. F. Molisch, N. Ashrafi, S. Ashrafi, *Adv. Opt. Photonics* **2015**, *7*, 66.
- [49] E. Maguid, I. Yulevich, D. Veksler, V. Kleiner, M. L. Brongersma, E. Hasman, *Science* **2016**, *352*, 1202.
- [50] S. Chen, Y. Zhang, Z. Li, H. Cheng, J. Tian, *Adv. Opt. Mater.* **2019**, *7*, 1801477.
- [51] H. Cheng, Z. Liu, S. Chen, J. Tian, *Adv. Mater.* **2015**, *27*, 5410.
- [52] M. Manjappa, P. Pitchappa, N. Singh, N. Wang, N. I. Zheludev, C. Lee, R. Singh, *Nat. Commun.* **2018**, *9*, 4056.
- [53] E. Maguid, I. Yulevich, M. Yannai, V. Kleiner, M. L. Brongersma, E. Hasman, *Light: Sci. Appl.* **2017**, *6*, e17027.
- [54] Y. Li, X. Li, L. Chen, M. Pu, J. Jin, M. Hong, X. Luo, *Adv. Opt. Mater.* **2017**, *5*, 1600502.
- [55] H. Zhao, B. Quan, X. Wang, C. Gu, J. Li, Y. Zhang, *ACS Photonics* **2018**, *5*, 1726.
- [56] W. Liu, Z. Li, Z. Li, H. Cheng, C. Tang, J. Li, S. Chen, J. Tian, *Adv. Mater.* **2019**, *31*, 1901729.
- [57] W. Liu, Z. Li, H. Cheng, S. Chen, J. Tian, *Phys. Rev. Appl.* **2017**, *8*, 014012.
- [58] Z. H. Jiang, L. Kang, W. Hong, D. H. Werner, *Phys. Rev. Appl.* **2018**, *9*, 064009.
- [59] J. Jin, M. Pu, Y. Wang, X. Li, X. Ma, J. Luo, Z. Zhao, P. Gao, X. Luo, *Adv. Mater. Technol.* **2017**, *2*, 1600201.
- [60] C. Zhang, F. Yue, D. Wen, M. Chen, Z. Zhang, W. Wang, X. Chen, *ACS Photonics* **2017**, *4*, 1906.
- [61] Y. Zhang, X. Yang, J. Gao, *Sci. Rep.* **2018**, *8*, 4884.
- [62] W. T. Chen, A. Y. Zhu, V. Sanjeev, M. Khorasaninejad, Z. Shi, E. Lee, F. Capasso, *Nat. Nanotechnol.* **2018**, *13*, 220.
- [63] G. Zheng, H. Mühlenbernd, M. Kenney, G. Li, T. Zentgraf, S. Zhang, *Nat. Nanotechnol.* **2015**, *10*, 308.
- [64] F. Yue, D. Wen, C. Zhang, B. D. Gerardot, W. Wang, S. Zhang, X. Chen, *Adv. Mater.* **2017**, *29*, 1603838.
- [65] M. Farmahini-Farahani, H. Mosallaei, *Opt. Lett.* **2013**, *38*, 462.
- [66] S. Liu, T. J. Cui, Q. Xu, D. Bao, L. Du, X. Wan, W. X. Tang, C. Ouyang, X. Y. Zhou, H. Yuan, H. F. Ma, W. X. Jiang, J. Han, W. Zhang, Q. Cheng, *Light: Sci. Appl.* **2016**, *5*, e16076.
- [67] T. J. Cui, M. Q. Qi, X. Wan, J. Zhao, Q. Cheng, *Light: Sci. Appl.* **2014**, *3*, e218.
- [68] Z. W. Xie, T. Lei, G. Y. Si, X. Y. Wang, J. Lin, C. J. Min, X. C. Yuan, *ACS Photonics* **2017**, *4*, 2158.
- [69] S. Chen, Z. Li, Y. Zhang, H. Cheng, J. Tian, *Adv. Opt. Mater.* **2018**, *6*, 1800104.
- [70] Z. Li, W. Liu, H. Cheng, S. Chen, J. Tian, *Adv. Opt. Mater.* **2017**, *5*, 1700413.
- [71] D. Wen, S. Chen, F. Yue, K. Chan, M. Chen, M. Ardron, K. Li, P. W. Wong, K. W. Cheah, E. Y. Pun, G. Li, S. Zhang, X. Chen, *Adv. Opt. Mater.* **2016**, *4*, 321.
- [72] Z. Zhang, D. Wen, C. Zhang, M. Chen, W. Wang, S. Chen, X. Chen, *ACS Photonics* **2018**, *5*, 1794.
- [73] D. Wen, F. Yue, G. Li, G. Zheng, K. Chan, S. Chen, M. Chen, K. F. Li, P. W. Wong, K. W. Cheah, E. Y. Pun, S. Zhang, X. Chen, *Nat. Commun.* **2015**, *6*, 8241.
- [74] M. Khorasaninejad, W. T. Chen, A. Y. Zhu, J. Oh, R. C. Devlin, D. Rousso, F. Capasso, *Nano Lett.* **2016**, *16*, 4595.
- [75] X. Chen, M. Chen, Q. Mehmood Muhammad, D. Wen, F. Yue, C. W. Qiu, S. Zhang, *Adv. Opt. Mater.* **2015**, *3*, 1201.
- [76] T. Cai, G. M. Wang, S. W. Tang, H. X. Xu, J. W. Duan, H. J. Guo, F. X. Guan, S. L. Sun, Q. He, L. Zhou, *Phys. Rev. Appl.* **2017**, *8*, 034033.
- [77] T. Cai, G. M. Wang, H. X. Xu, S. W. Tang, H. P. Li, J. G. Liang, Y. Q. Zhuang, *Ann. Phys.* **2018**, *530*, 1700321.
- [78] W. K. Pan, T. Cai, S. W. Tang, L. Zhou, J. F. Dong, *Opt. Express* **2018**, *26*, 17447.
- [79] Z. Li, W. Liu, H. Cheng, D. Y. Choi, S. Chen, J. Tian, *Adv. Opt. Mater.* **2019**, *7*, 1900260.
- [80] Y. W. Huang, W. T. Chen, W. Y. Tsai, P. C. Wu, C. M. Wang, G. Sun, D. P. Tsai, *Nano Lett.* **2015**, *15*, 3122.
- [81] B. Wang, F. Dong, Q. T. Li, D. Yang, C. Sun, J. Chen, Z. Song, L. Xu, W. Chu, Y. F. Xiao, Q. Gong, Y. Li, *Nano Lett.* **2016**, *16*, 5235.
- [82] B. Wang, F. Dong, D. Yang, Z. Song, L. Xu, W. Chu, Q. Gong, Y. Li, *Optica* **2017**, *4*, 1368.
- [83] O. Avayu, E. Almeida, Y. Prior, T. Ellenbogen, *Nat. Commun.* **2017**, *8*, 14992.
- [84] X. Wang, J. Ding, B. Zheng, S. An, G. Zhai, H. Zhang, *Sci. Rep.* **2018**, *8*, 1876.
- [85] J. Ding, N. Xu, H. Ren, Y. Lin, W. Zhang, H. Zhang, *Sci. Rep.* **2016**, *6*, 34020.
- [86] H. Yang, G. H. Li, G. T. Ca, F. L. Yu, Z. Y. Zhao, K. Ou, X. S. Chen, W. Lu, *Opt. Mater. Express* **2018**, *8*, 1940.
- [87] A. Forouzmmand, H. Mosallaei, *ACS Photonics* **2018**, *5*, 1427.
- [88] H. Cheng, X. Wei, P. Yu, Z. Li, Z. Liu, J. Li, S. Chen, J. Tian, *Appl. Phys. Lett.* **2017**, *110*, 171903.
- [89] W. Ma, F. Cheng, Y. M. Liu, *ACS Nano* **2018**, *12*, 6326.
- [90] Z. Li, W. Liu, Z. Li, C. Tang, H. Cheng, J. Li, X. Chen, S. Chen, J. Tian, *Laser Photonics Rev.* **2018**, *12*, 1800164.
- [91] M. Ma, Z. Li, W. Liu, C. Tang, Z. Li, H. Cheng, J. Li, S. Chen, J. Tian, *Laser Photonics Rev.* **2019**, *13*, 1900056.
- [92] S. M. Kamali, E. Arbabi, A. Arbabi, Y. Horie, M. Faraji-Dana, A. Faraon, *Phys. Rev. X* **2017**, *7*, 041056.
- [93] Z. -L. Deng, Y. Cao, X. Li, G. P. Wang, *Photonics Res.* **2018**, *6*, 443.
- [94] M. Qiu, M. Jia, S. Ma, S. L. Sun, Q. He, L. Zhou, *Phys. Rev. Appl.* **2018**, *9*, 054050.
- [95] Y. Bao, Y. Yu, H. Xu, Q. Lin, Y. Wang, J. Li, Z. K. Zhou, X. H. Wang, *Adv. Funct. Mater.* **2018**, *28*, 1805306.
- [96] C. H. Chu, M. L. Tseng, J. Chen, P. C. Wu, Y. H. Chen, H. C. Wang, T. Y. Chen, W. T. Hsieh, H. J. Wu, G. Sun, D. P. Tsai, *Laser Photonics Rev.* **2016**, *10*, 986.
- [97] L. B. Yan, W. M. Zhu, P. C. Wu, H. Cai, D. Gu, L. K. Chin, Z. X. Shen, P. H. J. Chong, Z. C. Yang, W. Ser, D. P. Tsai, A. Q. Liu, *Appl. Phys. Lett.* **2017**, *110*, 201904.
- [98] J. Li, S. Kamin, G. Zheng, F. Neubrech, S. Zhang, N. Liu, *Sci. Adv.* **2018**, *4*, eaar6768.
- [99] X. Yin, T. Steinle, L. Huang, T. Taubner, M. Wuttig, T. Zentgraf, H. Giessen, *Light: Sci. Appl.* **2017**, *6*, e17016.
- [100] P. Yu, J. Li, S. Zhang, Z. Jin, G. Schutz, C. W. Qiu, M. Hirscher, N. Liu, *Nano Lett.* **2018**, *18*, 4584.
- [101] X. Duan, N. Liu, *ACS Nano* **2018**, *12*, 8817.
- [102] C. Wang, W. Liu, Z. Li, H. Cheng, Z. Li, S. Chen, J. Tian, *Adv. Opt. Mater.* **2018**, *6*, 1701047.
- [103] Z. Li, W. Liu, H. Cheng, S. Chen, J. Tian, *Opt. Lett.* **2016**, *41*, 3142.
- [104] H. Cheng, S. Chen, P. Yu, W. Liu, Z. Li, J. Li, B. Xie, J. Tian, *Adv. Opt. Mater.* **2015**, *3*, 1744.
- [105] J. Li, P. Yu, H. Cheng, W. Liu, Z. Li, B. Xie, S. Chen, J. Tian, *Adv. Opt. Mater.* **2016**, *4*, 91.
- [106] Y. Zhang, Z. Li, W. Liu, Z. Li, H. Cheng, S. Chen, J. Tian, *Adv. Opt. Mater.* **2019**, *7*, 1801273.
- [107] Z. Li, M. H. Kim, C. Wang, Z. Han, S. Shrestha, A. C. Overvig, M. Lu, A. Stein, A. M. Agarwal, M. Loncar, N. Yu, *Nat. Nanotechnol.* **2017**, *12*, 675.
- [108] B. Groever, W. T. Chen, F. Capasso, *Nano Lett.* **2017**, *17*, 4902.

- [109] A. Arbabi, E. Arbabi, S. M. Kamali, Y. Horie, S. Han, A. Faraon, *Nat. Commun.* **2016**, *7*, 13682.
- [110] Y. Li, S. Kita, P. Muñoz, O. Reshef, D. I. Vulis, M. Yin, M. Lončar, E. Mazur, *Nat. Photonics* **2015**, *9*, 738.
- [111] Y. Wang, X. Fang, Z. Kuang, H. Wang, D. Wei, Y. Liang, Q. Wang, T. Xu, Y. Zhang, M. Xiao, *Opt. Lett.* **2017**, *42*, 2463.
- [112] B. Shen, P. Wang, R. Polson, R. Menon, *Nat. Photonics* **2015**, *9*, 378.
- [113] S. Jahani, Z. Jacob, *Nat. Nanotechnol.* **2016**, *11*, 23.
- [114] P. Cheben, R. Halir, J. H. Schmid, H. A. Atwater, D. R. Smith, *Nature* **2018**, *560*, 565.
- [115] D. Lin, P. Fan, E. Hasman, M. L. Brongersma, *Science* **2014**, *345*, 298.
- [116] E. Arbabi, A. Arbabi, S. M. Kamali, Y. Horie, M. Faraji-Dana, A. Faraon, *Nat. Commun.* **2018**, *9*, 812.
- [117] Z. Dong, J. Ho, Y. F. Yu, Y. H. Fu, R. Paniagua-Dominguez, S. Wang, A. I. Kuznetsov, J. K. W. Yang, *Nano Lett.* **2017**, *17*, 7620.
- [118] M. Serra-Garcia, V. Peri, R. Susstrunk, O. R. Bilal, T. Larsen, L. G. Villanueva, S. D. Huber, *Nature* **2018**, *555*, 342.
- [119] C. Hu, Z. Li, R. Tong, X. Wu, Z. Xia, L. Wang, S. Li, Y. Huang, S. Wang, B. Hou, C. T. Chan, W. Wen, *Phys. Rev. Lett.* **2018**, *121*, 024301.